Article

Synthesis of Propylene Glycol Methyl Ether Acetate: Reaction Kinetics and Process Simulation Using Heterogeneous Catalyst

Yui Rak Son [1], Jong Kee Park [2], Eun Woo Shin [1], Seok Pyong Moon [3] and Heon E. Park [4,*]

[1] School of Chemical Engineering, University of Ulsan, 93 Daehak-ro, Nam-gu, Ulsan 44610, Republic of Korea; newson0@naver.com (Y.R.S.); ewshin@ulsan.ac.kr (E.W.S.)
[2] Korea Institute of Energy Research, 152 Gajeong-ro, Yuseong-gu, Daejeon 34129, Republic of Korea; jngkprk@kier.re.kr
[3] Samsung-BP Chemicals, 63-15, Sanggae-ro, Cheongryang-eup, Ulju-gun, Ulsan 44987, Republic of Korea; moonseokpyong82@gmail.com
[4] Department of Chemical and Process Engineering, University of Canterbury, Private Bag 4800, Ilam, Christchurch 8041, New Zealand
[*] Correspondence: heon.park@canterbury.ac.nz; Tel.: +64-3-369-0962

Abstract: Propylene glycol methyl ether acetate (PGMEA) serves as a crucial solvent in semiconductor and display material processes, demanding high purity and low acidity. Despite its significance, its conventional synthesis method using homogeneous catalysts requires extensive purification. Our study explores the use of Amberlyst-15, a stable solid catalyst, to streamline this process. Through batch reactions with a 1:1 reactant ratio at various temperatures and modeling using an integrated reaction rate equation, we obtained kinetic parameters. These parameters were used to predict the kinetics under different reactant ratios and different catalyst amounts, and the predictions match well with experimental results, especially when we used the catalyst amount scaled by the amount of the limiting reactant (PGME) rather than the total amount of the reactants. This highlights the importance of reporting kinetic parameters with proper scaling for catalyst used. Furthermore, we integrated these parameters into process simulations to determine the length of a plug flow reactor (PFR), constructed a PFR system, and confirmed that the simulation results matched well with experimental data obtained from the PFR system. Our findings suggest Amberlyst-15's potential in simplifying PGMEA synthesis, promising advancements in industrial applications.

Keywords: propylene glycol methyl ether acetate; methoxy propyl acetate; propylene glycol methyl ether; methoxy propanol; acetic acid; reaction kinetics; heterogeneous catalyst; Amberlyst-15; integrated reaction rate equation; pseudo-homogeneous; reaction rate constant; activation energy

1. Introduction

Propylene glycol methyl ether acetate (PGMEA), also known as PMA or methoxy propyl acetate, serves as a vital solvent with diverse applications across several industries. Its use ranges from electronic chemicals in semiconductor manufacturing to ultra-high purity applications [1], ultra-low acidity [2,3], and reduced toxicity compared to ethylene glycol-based products [4]. PGMEA is also used as a solvent in paints, inks, dyes, cleaning agents, and photoresists, making it a preferred choice due to its low toxicity profile and minimal particle formation. Notably, PGMEA is a key component in various coating formulations [5]. PGMEA synthesis primarily involves the esterification reaction of propylene glycol methyl ether (PGME or methoxy propanol) with acetic acid (AA). However, this process encounters challenges due to chemical equilibrium limitations, resulting in low PGME conversion rates. The synthesis reaction is represented by the following equilibrium equation:

$$\underset{\text{acetic acid}}{\overset{\text{A}}{\text{(AA)}}} + \underset{\text{PGME}}{\overset{\text{B}}{\text{(PGME)}}} \underset{k_r}{\overset{k_f}{\rightleftharpoons}} \underset{\text{PGMEA}}{\overset{\text{C}}{\text{(PGMEA)}}} + \underset{\text{water}}{\overset{\text{D}}{H_2O}} \tag{1}$$
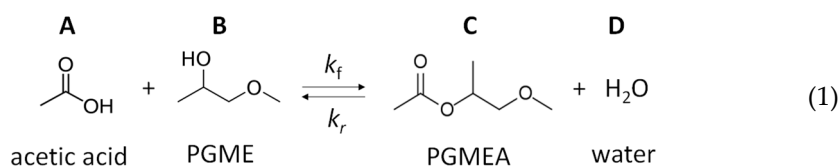
where k_1 and k_2 denote the forward and reverse reaction rate constants, respectively, and A through D are PGME, AA, PGMEA, and water, respectively. As an equilibrium reaction, it necessitates the use of an acidic catalyst to facilitate the reaction kinetics.

Homogeneous catalysts, such as sulfuric acid and hydrofluoric acid, have long been favored for their high catalytic activity and selectivity in various chemical reactions. However, their use comes with drawbacks, challenges in catalyst separation, process complexity, and corrosion issues. In contrast, heterogeneous acidic catalysts have emerged as promising alternatives due to their high catalytic activity, low corrosivity, and ease of separation [6,7]. Solid acids, in particular, have gained traction across a spectrum of chemical reactions, including esterification [8,9], alkanes isomerization [10], aldol condensation [11] and ketal reaction [12]. Their utility lies in their ability to enhance kinetics inherent in esterification reactions. Recent studies have introduced innovative methods, such as reactive distillation (RD) and pressure swing techniques, aimed at improving energy efficiency and reducing production costs in PGMEA synthesis [13,14]. The RD reaction process, comprising a transesterification reaction coupled with a distillation column for azeotrope separation and energy optimization, offers a viable solution to enhance the efficiency of esterification processes [4,15].

Furthermore, the availability of heterogeneous catalysts enables the production of less-acidic electronic-grade PGMEA, contributing to the enhancement of product quality [2–4]. Amberlyst® 15 (Amberlyst-15) is a widely used catalyst in various chemical processes, renowned for its excellent physical, thermal, and chemical stability [16]. Available in bead form, Amberlyst-15 is insoluble in water, making it suitable for non-aqueous catalysis—a crucial aspect, particularly in reactions where water is a byproduct and catalyst dissolution is undesirable. On the other hand, this catalyst can dissolve or swell in other types of liquid. For example, Amberlryst-15 will swell in acetone, so this catalyst should be used in reactions where the environment is favorable for the catalyst. Its proven stability in harsh environments, including acidic conditions, makes it an attractive option for catalytic reactions. Despite its established stability and compatibility, only limited studies have explored the use of Amberlyst-15 in synthesizing PGMEA. Further investigation into its catalytic performance in PGMEA synthesis could unveil its potential benefits.

Oh et al. [17] conducted PGMEA synthesis with Amberlyst-15 catalyst using a batch system, exploring various [PGME]:[AA] ratios and temperatures to determine reaction kinetics. Subsequently, they applied these findings to design and operate reactive distillation processes. Despite observing two reaction sites inside the column with larger injection volumes, their study achieved nearly 100% conversion at lower flow rates and smaller injection volumes. However, the batch system model fitting was not sufficiently robust, warranting further clarification of parameter determination methods. Gadekar-Shinde et al. [4] proposed an RD process for PGMEA production, exploring reaction rates at different temperatures and reactant mole ratios. They introduced toluene as an entrainer to enhance product purity without compromising catalyst stability, presenting a more compact and cost-effective process. Agrawal et al. [2] optimized a simulated moving bed reactor (SMBR) for PGMEA synthesis using Amberlyst-15. Their model revealed that increased AA conversion negatively impacted PGMEA production rates, emphasizing the importance of process operation for high PGMEA recovery and reduced downstream separation costs. Utilizing kinetic model parameters from previous studies, they optimized the SMBR, observing similar phenomena of two reaction sites and enhanced conversion beyond equilibrium in chromatograph reactors.

Huang et al. [18] investigated the synthesis of PGMEA using a solid acidic catalyst (SO_4^{2-}/TiO_2) and optimized its preparation. Their study demonstrated the catalyst's high stability and consistent performance. Oh et al. [3] and Wang et al. [15] explored PGMEA synthesis via transesterification reactions using different catalysts, observing varying conversion rates and catalyst deactivation. Wang et al. [15] utilized kinetic data to design and operate RD systems while Oh et al. [3] investigated the synthesis of PGMEA using ethyl acetate instead of acetic acid as a precursor. Fan et al. [13] investigated PGMEA synthesis via transesterification of methyl acetate and PGME using an RD process. They provided transesterification kinetics and thermodynamic parameters, validating the reaction feasibility experimentally in a batch RD column.

In this study, we utilized Amberlyst-15, with the aim of determining its reaction kinetics and investigating its applicability in continuous processes based on the kinetics. The catalyst was used in its commercially available form without any additional chemical treatment, mirroring common industrial practices. Our experimental approach involved studying the reaction kinetics of the process described in Equation (1) across a range of temperatures (60 to 100 °C) using a 1:1 ratio of PGME to AA and a fixed amount of Amberlyst-15 in a batch system. We developed an integrated reaction rate model, which was not available in previous studies, and extracted kinetic model parameters, including Arrhenius parameters, from the experimental data. Subsequently, we conducted additional experiments with different PGME to AA ratios and varied amounts of Amberlyst-15, comparing the resulting data with model predictions based on the earlier determined kinetic parameters. To account for the influence of catalyst amount on the reaction rate constant, we scaled the kinetic parameters using two distinct methods of expressing catalyst amount and showed which method is better. Finally, we employed the determined kinetic parameters to simulate the behavior of a plug flow reactor, informing the design process for reactor systems in potential industrial applications. Our study provides insights into the reaction kinetics of the PGME and AA synthesis process and highlights the potential utility of Amberlyst-15 as a catalyst in industrial settings. The novel features of this study are providing kinetic parameters with an explicit reaction equation, which are readily usable for designing reaction systems for PGMEA and suggesting the method to scale the amount of catalyst for better model predictions. Future research directions may involve further validation of the proposed kinetic model and exploration of alternative catalyst formulations for enhanced reaction efficiency.

2. Materials and Methods

All materials used were of laboratory reagent grade and employed without further purification. PGMEA (>99.5%), PGME (>99.5%), AA (>99.7%), and methanol (>99.9%) were procured from Sigma-Aldrich (St. Louis, MO, USA). The solid catalyst, Amberlyst® 15 hydrogen form (Amberlyst-15), was also obtained from Sigma-Aldrich (St. Louis, MO, USA). Helium (>99.999%) was supplied by Deokyang (Ulsan, Republic of Korea), and nitrogen (>99.8%) was provided by Air Products (Pyeongtaek, Republic of Korea).

Figure 1 illustrates the batch reaction system utilized to determine the reaction kinetics. The round-bottom flask has a 2 L volume with a 3-neck apparatus including a reflux condenser, heater, and magnetic stirrer. It also features a temperature controller and a sampling port, through which sampling took place regularly using a syringe with a needle. To minimize the loss of reactants and products during experiments, chilled water at 5 °C was circulated through the reflux condenser. We took a specified mass of each reactant, AA and PGME, to achieve a desired reactant ratio, along with approximately a 1 kg total mass. Each component was then introduced into the batch reactor accordingly. The ratio of the reactants varied for different tests. The reactor's temperature was controlled to one of five predetermined temperatures: 60, 70, 80, 90, or 100 °C. Upon reaching the designated reaction temperature, a desired amount of catalyst was added to initiate the reaction. Stirring of the reaction mixture at 300 rpm commenced immediately after cata-

lyst addition, with the stirring speed chosen based on previous studies indicating its minimal impact on reaction kinetics, especially the concentration of PGMEA [17]. Samples were extracted from the reactor at specified time intervals to monitor the reaction progress. It was assumed that the reaction ceased in the sample due to the absence of catalyst. Gas chromatography (GC) analysis using a Varian CP3800 (Palo Alto, CA, USA) equipped with a flame ionization detector (FID) was employed to determine the composition of each sample. The GC conditions, summarized in Table 1, included parameters such as column temperature, injection volume, and carrier gas flow rate. Before conducting the experiment, an external calibration was conducted using the same chemicals (AA, PGME, and PGMEA) with known concentrations. The resulting calibration curve was utilized to determine the concentrations of these chemicals during the experiments. No internal standard was employed. An example of chromatogram is shown in the Supplementary Materials.
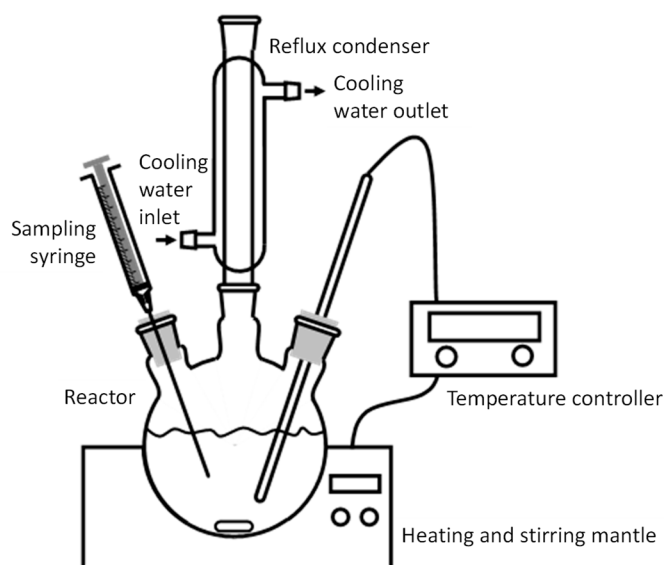
Figure 1. Schematic of batch reaction system.

Table 1. Operating conditions for GC.

Conditions	Value
Capillary column	DB-FFAP (length: 30 m, diameter: 0.25 mm, film: 0.25 μm)
Injector temperature	230 °C
Split ratio	10:1
Dilution	[methanol]/[sample] = 10:1
Oven temperature	Keep at 50 °C for 5 min, increase at 30 °C/min, and keep at 230 °C for 5 min
Detector temperature	230 °C
He carrier	689.5 mbar, 1.0 mL/min

We conducted simulations using Aspen Plus 2006.5, employing a reactor model of RPLUG. Our aim was to design a plug flow reactor (PFR) by integrating kinetic parameters obtained from the batch system experiments performed in this investigation. The simulations were carried out at a temperature of 90 °C, with the bed porosity and density of the catalyst particles set at 0.3 and 0.5 g/cc, respectively. The reactor dimensions were specified with a diameter of 0.1 m and a length of 1.5 m. The flowsheet and conditions are detailed in the Supplementary Materials. Accordingly, a PFR system (Figure 2) was constructed, comprising a PFR reactor with dimensions of 0.1 m in diameter and 1.5 m in length. We replicated identical operational conditions to those used in the simulation to

obtain the mole fractions of PGME and PGMEA at two sampling locations along the PFR: 0.5 m and 1.5 m (i.e., outlet) to compare the simulation and experimental results.

Figure 2. PFR system with the same dimensions used in simulation.

3. Kinetic Modeling

Activity coefficients, often estimated using UNIQUAC or UNIFAC methods, are utilized to correct for deviations from ideal behavior [19–21]. For instance, Popken et al. [22] demonstrated that utilizing activities obtained from UNIQUAC calculations, rather than mole fractions, provided a better representation of experimental values in the synthesis of methyl acetate using Amberlyst-15. Despite the prevalence of activity-based models, kinetic models frequently rely on concentrations rather than activities [23–26]. In our study, we adopted liquid concentrations (i.e., mole fractions) in the development of our kinetic model for simplicity, with a discussion of its predictive capabilities to follow.

We employed a pseudo-homogeneous model [22], assuming the ion-exchange resin serves as a source of solvated protons. The differential molar balance governing the formation of PGMEA can be expressed as a second-order kinetic model, representing a first-order reaction with respect to each component. For our reversible reaction system, the reaction rate is modeled as

$$-r_A = \frac{d[\text{A}]}{dt} = k_1[\text{A}][\text{B}] - k_2[\text{C}][\text{D}] \tag{2}$$

where [i] (mol/L) is the concentration of a component i, (A, B, C, or D), as a function of time, and subscripts 1 and 2 denote forward and reverse reactions, respectively. The forward and reverse reaction rate constants, k_1 and k_2, are expressed in units of L/(mol min). The concentration of each component in the reaction system was determined at 20 °C within the total volume of all components, which amounted to 1034 mL. The equilibrium constant, K_e, is defined as the ratio of the forward and reverse reaction rate constants at equilibrium and can be expressed as

$$K_e \equiv \frac{k_1}{k_2} = \frac{[\text{C}]_e[\text{D}]_e}{[\text{A}]_e[\text{B}]_e} \tag{3}$$

where the subscript e denotes equilibrium.

For the general case of $[\text{A}]_0 \leq [\text{B}]_0$, we can derive the integrated rate equation for Equation (1), i.e., the concentration of a component at a certain time during the reaction

$$[\text{A}](t) = \frac{a - z(t)b}{1 - z(t)} \tag{4}$$

where z, a, and b are defined as

$$z(t) \equiv \left(\frac{[A]_0 - a}{[A]_0 - b}\right) \exp[t(k_2 - k_1)(a - b)] \tag{5}$$

$$a \equiv \frac{-(k_1[A]_0 - k_1[B]_0 - 2k_2[A]_0) + \sqrt{(k_1[A]_0 - k_1[B]_0 - 2k_2[A]_0)^2 - 4(k_2 - k_1)k_2[A]_0^2}}{2(k_2 - k_1)} \tag{6}$$

$$b \equiv \frac{-(k_1[A]_0 - k_1[B]_0 - 2k_2[A]_0) - \sqrt{(k_1[A]_0 - k_1[B]_0 - 2k_2[A]_0)^2 - 4(k_2 - k_1)k_2[A]_0^2}}{2(k_2 - k_1)} \tag{7}$$

where $[A]_0$ and $[B]_0$ are the initial concentrations of components A and B, respectively. Then, the concentration of the other components at a certain time can be modeled as follows:

$$[B] = [B]_0 - ([A]_0 - [A]) \tag{8}$$

$$[C] = [D] = [A]_0 - [A] \tag{9}$$

We used $[A]_0$ and $[B]_0$ and measured $[A]_e$ and $[B]_e$ to calculate a, b, and $z(t)$ with an initial guess of k_1 and eventually to obtain model $[A](t)$ (Equation (4)). Using the least square method to minimize the sum of squared error, which is the difference between model $[A](t)$ and data $[A](t)$, k_1 was obtained (and naturally k_2 as well).

For the case of $[A]_0 = [B]_0$, while Equations (4) and (5) can be used as those are, Equations (6) and (7) simplify to

$$a = \frac{k_2 A_0 + \sqrt{k_1 k_2 [A]_0^2}}{k_2 - k_1} \tag{10}$$

$$b = \frac{k_2 A_0 - \sqrt{k_1 k_2 [A]_0^2}}{k_2 - k_1} \tag{11}$$

Equations (3) through (5) and (8) through (11) were utilized to determine the reaction rate constants by fitting experimental data obtained with a reactants' mole ratio of 1:1 at various temperatures to the model represented by Equation (4). This fitting assumed a pseudo-homogeneous reaction. Subsequently, the same reaction rate constants and Equations (3) through (9) were employed to forecast the reaction kinetics with a reactants' mole ratio other than 1:1, thereby validating the previously determined reaction rate constants.

The scaled forward and reverse reaction rate constants are expressed in units of L mol-PGME/(mol min g-catalyst). These constants are calculated using the following equations:

$$k_f \equiv k_1/m_{cat} \tag{12}$$

$$k_r \equiv k_2/m_{cat} \tag{13}$$

where m_{cat} in g-catalyst/mol-reactant is the catalyst amount relative to the number of moles of reactant (either total or limiting reactant). The scaled reaction rate constants k_f and k_r should remain unchanged regardless of the specific amount of catalyst utilized in the reaction system. As long as the reactant amount is used consistently, whether it is divided by the total amount of all the reactants or the amount of the limiting reactant, these constants can be universally applied across different catalyst amounts without alteration. For reactions involving a different amount of catalyst, the prediction can be made using Equation (4) with the following updated reaction rate constants:

$$k_1' = k_f \times m_{cat}' \tag{14}$$

where m_{cat}' in g-catalyst/mol-reactant is the new amount of catalyst different from that used in this study, k_1' in L/(mol min) represents the new forward reaction rate constant for the catalyst amount, and k_f in L mol-PGME/(mol min g-catalyst) is the scaled forward

reaction rate constant determined in this study. The new reverse reaction rate constant can be obtained by

$$k_2' = \frac{k_1'}{K_e'} \tag{15}$$

where K_e' is the equilibrium constant obtained in the reaction with the catalyst amount, m_{cat}'. Thus, Equation (4) should be reduced to the following universal equation:

$$-r_A = \frac{d[\text{A}]}{dt} = k_f m_{cat}'[\text{A}][\text{B}] - k_r m_{cat}'[\text{C}][\text{D}] \tag{16}$$

Again, Equations (5) through (9) and (16) were employed to forecast the reaction kinetics with catalyst amounts different from what used to determine k_f and k_r, thereby validating the previously determined reaction rate constants.

The effect of temperature on the reaction rate constants can be described by the Arrhenius equation:

$$k_1 = A_1 e^{-\frac{E_{a,1}}{RT}} \tag{17}$$

$$k_2 = A_2 e^{-\frac{E_{a,2}}{RT}} \tag{18}$$

$$k_f = A_f e^{-\frac{E_{a,1}}{RT}} \tag{19}$$

$$k_r = A_r e^{-\frac{E_{a,2}}{RT}} \tag{20}$$

where $E_{a,1}$ and $E_{a,2}$ (J/mol) represent the activation energies for the forward and reverse reactions, respectively, R is the gas constant, equal to 8.31446 J/(mol K), A_1 and A_2 in L/(mol min) are the pre-exponential factors for the forward and reverse reaction rate constants, respectively, and A_f and A_r in L mol-PGME/(mol min g-catalyst) are the pre-exponential factors for the scaled forward and reverse reaction rate constants, respectively, as follows:

$$A_f = A_1/m_{cat}' \tag{21}$$

$$A_r = A_2/m_{cat}' \tag{22}$$

4. Results and Discussion

### 4.1. Effect of Temperature and Kinetic Parameters

First, we conducted PGMEA synthesis reactions with a 1:1 reactants mole ratio (i.e., $[\text{PGME}]_0 = [\text{AA}]_0$) at various temperatures. Figure 3 illustrates the effect of temperature on the concentration of PGME and the product PGMEA with time at five different temperatures ranging from 60 to 100 °C with a catalyst amount of 14.5 g-catalyst/mol-PGME (equivalent to 7.3 g-catalyst/mol-reactants or 0.1 g-catalyst/mL-reactants). The experiments were conducted over a significantly longer duration than depicted in Figure 3. However, for brevity and clarity, we present data only up to concentrations equivalent to those observed at later times when there was no more change in the concentrations. Consequently, the final concentrations depicted represent the equilibrium compositions. As expected, higher temperatures lead to shorter times to reach equilibrium, consistent with the well-known effect of temperature on reaction rates. The equilibrium concentrations of each reactant are approximately equal to that of the product, i.e., $K_e \approx 1$.

Equations (3) through (5) and (8) through (11) were utilized to determine the reaction rate constants by fitting the data obtained with a reactants' mole ratio of 1:1 to the model, Equation (4), assuming a pseudo-homogeneous reaction. Figure 3 also presents the model predictions for both PGME and PGMEA. The former was obtained using Equation (4),

while the latter was obtained using Equations (4) and (9). Generally, the data align well with the model predictions. The reaction rate constants as a function of temperature were naturally obtained and are depicted in Figure 4. These data were fitted to Equations (17) and (18) to determine the activation energy and pre-exponential factors. The resulting values are tabulated in Table 2.

The reverse reaction rate constants tend to be higher than the forward reaction constants within the range of operating temperatures, except at 60 °C, where both rates are about the same. However, the activation energy for the reverse reaction is higher than that for the forward reaction, suggesting that the reaction rates of the reverse reaction are more temperature-sensitive compared to the forward reaction. Thus, at lower temperatures, such as 50 °C or below, we anticipate that the forward reaction rate will exceed that of the reverse reaction, leading to higher conversion rates.
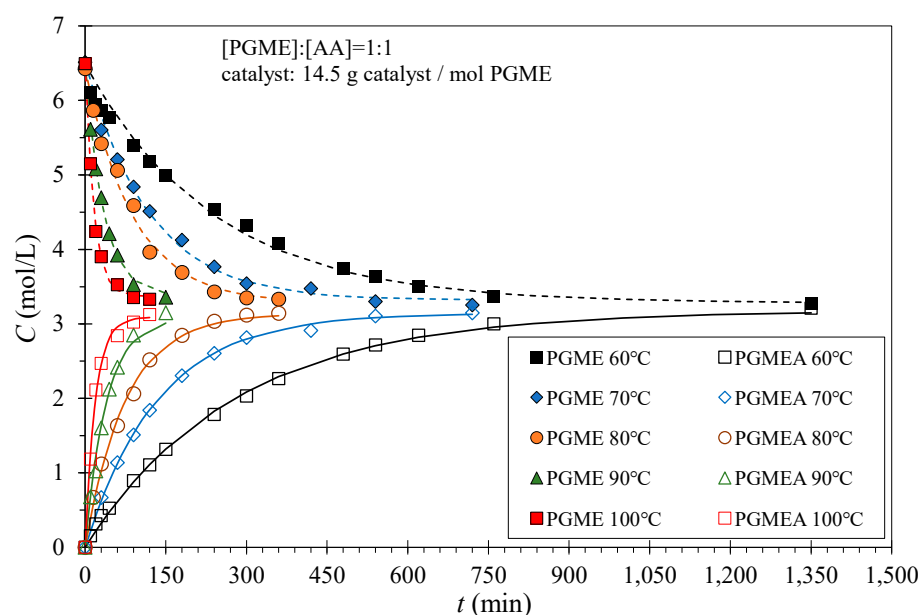
Figure 3. Effects of temperature and time on the concentrations (C) of PGME and PGMEA during reaction with 14.5 g catalyst/mol PGME, which is equivalent to 7.3 g catalyst/mol reactants or 0.1 g catalyst/mL reactants. Dashed lines are model predictions, Equation (4), for PGME, while solid lines are model predictions, Equations (4) and (9), for PGMEA. Data and predictions after reaching equilibrium are not shown to avoid confusion.
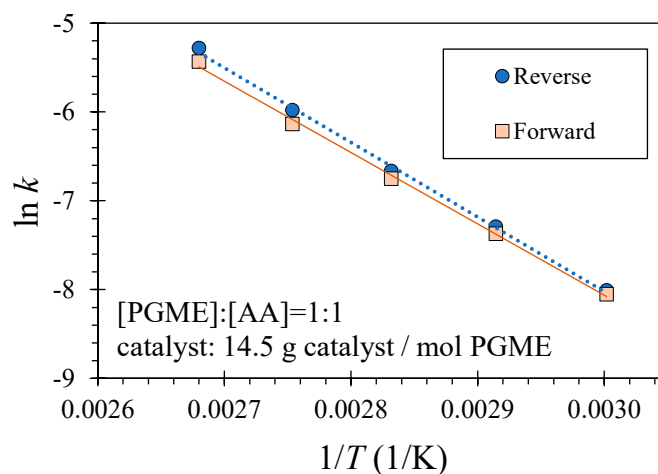
Figure 4. Effects of temperature on the forward and reverse reaction rate constants in L/(mol min). The lines are Arrhenius model predictions, Equations (17) and (18), with $R^2 = 0.9981$ and $R^2 = 0.9984$ for forward and reverse reactions, respectively.

Table 2. Parameters of reaction kinetics.

		Forward				Reverse		
Source	$E_{a,1}$	A_1	A_f^*	A_f^+	$E_{a,2}$	A_2	A_r^*	A_r^+
This study	66.86	9.40×10^6	6.46×10^5	1.28×10^6	71.45	2.95×10^7	2.03×10^6	4.0×10^6
Huang et al. [18]	65.68	6.84×10^5			57.78	8.0×10^5		
Oh et al. [17]	61.59							
Gadekar-Shinde et al. [4]	66.50			1.73×10^6 ++	24.88			1.83 ++

$E_{a,1}$ and $E_{a,2}$ are in $\frac{\text{kJ}}{\text{mol}}$; A_1 and A_2 are in $\frac{\text{L}}{\text{mol min}}$; A_f^* and A_r^* are in $\left(\frac{\text{L}}{\text{mol min}}\right)\left(\frac{\text{mol}-\text{PGME}}{\text{g}-\text{catalyst}}\right)$; A_f^+ and A_r^+ are in $\left(\frac{\text{L}}{\text{mol min}}\right)\left(\frac{\text{mol}-\text{reactants}}{\text{g}-\text{catalyst}}\right)$; ++: converted the original value for consistent units.

It is intriguing to juxtapose our findings with those of other researchers using a similar system. Huang et al. [18] obtained kinetic parameters at higher temperatures than those investigated in this study. Notably, their reported reaction rate constants are not scaled with the catalyst amount. Thus, Figure 5 presents a comparison for the forward reaction rate constant without scaling, expressed in units of L/(min mol). Generally, the rate constants obtained in our study are higher than those reported by Huang et al. [18] even though those have the same order of magnitude. While those studies show different reaction rate constants, both datasets exhibit similar slopes, indicating comparable activation energies (Table 2).

On the other hand, Oh et al. [17] and Gadekar-Shinde et al. [4] did not explicitly detail how their reaction rate constants were scaled, making a direct comparison challenging. However, it is important to note that the method of scaling should primarily affect the pre-exponential factor rather than the activation energy. As shown in Table 2, the activation energy for the forward reaction remains consistent across the four studies, while that for the reverse reaction displays considerable variation. Particularly, Gadekar-Shinde et al. [4] reported a notably low activation energy for the reverse reaction, achieving high conversions. Their methodology involved stirring the reaction mixture at a significantly higher rate than in our study to minimize mass transfer resistance. Additionally, they applied chemical treatment to the catalyst, which could account for the observed differences. The challenge of achieving high conversion in esterification is closely tied to the removal of water from the reaction mixture, as water is one of the products in this reversible reaction. Le Chatelier's principle predicts that removing water will drive the equilibrium towards the formation of products, thus enhancing conversion. Additionally, modifying the catalyst through chemical treatments can also induce changes in its chemistry, further influencing the reaction dynamics. However, the implementation of an additional chemical treatment facility can be costly. Moreover, stirring the reaction mixture at high speeds in an industrial setting can pose risks. Considering these factors, along with the potential for uncontrolled mass transfer resistance in a plug flow reactor (PFR), we chose a lower stirring speed that does not influence the reaction [17], and furthermore, we used the catalyst in its original state without any chemical treatment. Our aim was to provide reaction kinetic parameters applicable to similar industrial setups.
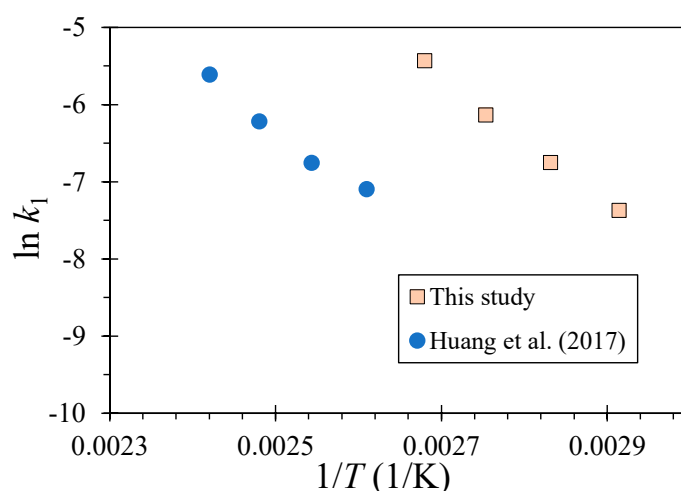
Figure 5. Comparison of the forward reaction rate constant for the case of [PGME]:[AA] = 1:1 in this study with a similar study [18].

4.2. Validation of Kinetic Parameters with Various Initial Concentrations and Catalyst Amount

It is crucial to assess whether the parameters for reaction kinetics obtained in the previous section for the 1:1 reactant mole ratio are still applicable for other reactant mole ratios and different catalyst amounts. Figure 6a displays the concentration profiles of two reactants and PGMEA over time for a [PGME]:[AA] ratio of 1:4 with 37 g-catalyst/mol-PGME at 80 °C. The model predictions are based on Equations (3) through (9) using the same scaled reaction rate constants (k_f) derived in the previous section for the 1:1 reactant mole ratio with 14.5 g-catalyst/mol-PGME at the same temperature. The new reaction rate constants were obtained using Equations (14) and (15). Similarly, Figure 6b depicts the concentration profiles for a [PGME]:[AA] ratio of 1:2 with 20 g-catalyst/mol-PGME at 100 °C. The predictions were obtained using the same approach. Generally, the model predicts the behavior quite accurately despite changes in both the reactant ratio and catalyst amount. These results suggest that the kinetic parameters (k_f and thus A and E_a) can be universally applied to design reactors or predict reaction kinetics without using the activity coefficient.

The catalyst amount should impact kinetics rather than equilibrium, influencing the time required to reach equilibrium [18]. Therefore, the method of scaling the reaction rate constant will affect predictions on the time axis. A pertinent question arises regarding the optimal way to scale with the catalyst amount: should it be relative to the total amount of the reactants or the amount of the limiting reactant (PGME in this study)? Figure 6a,b, based on the former case, indicate predictions slower than the data in terms of time to reach equilibrium. Conversely, Figure 6c,d, based on the latter case, show predictions faster than the former case. When employing a specific catalyst mass for two different reactions—one with a limiting reactant and the other with a 1:1 reactant ratio—while maintaining the same total number of moles of reactants, the catalyst amount per the limiting reactant in the former case will appear higher than that in the latter case even though the catalyst amount per the total amount of reactants is the same for both cases. Since the reaction is controlled by the limiting reactant, the reaction should proceed faster from the limiting reactant's perspective in the former case compared to the reaction with a 1:1 reactant ratio if the absolute amount of catalyst remains constant. Thus, while kinetic data in Figure 6a,b outpace the model predictions using the catalyst amount calculated based on the total amount of reactants, the predictions using the catalyst amount calculated based on the amount of the limiting reactant as shown in Figure 6c,d better align with the data. Therefore, when reporting or using parameters for reaction kinetics, the pre-exponential factor or reaction rate constants scaled with the catalyst amount per the amount of the limiting reactant need to be reported or used. Thus, m_{cat} and m'_{cat} in Equations (12) through (14), (16), (21), and (22) should be as follows:

$$m_{cat} = \frac{\text{mass of catalyst}}{\text{moles of limiting reactant}} \tag{23}$$

and

$$m'_{cat} = \frac{\text{mass of catalyst}}{\text{moles of limiting reactant}} \tag{24}$$

This naturally leads to using A_f^* and A_r^* instead of A_f^+ and A_r^+ in Table 2 to predict kinetics or design a reactor.
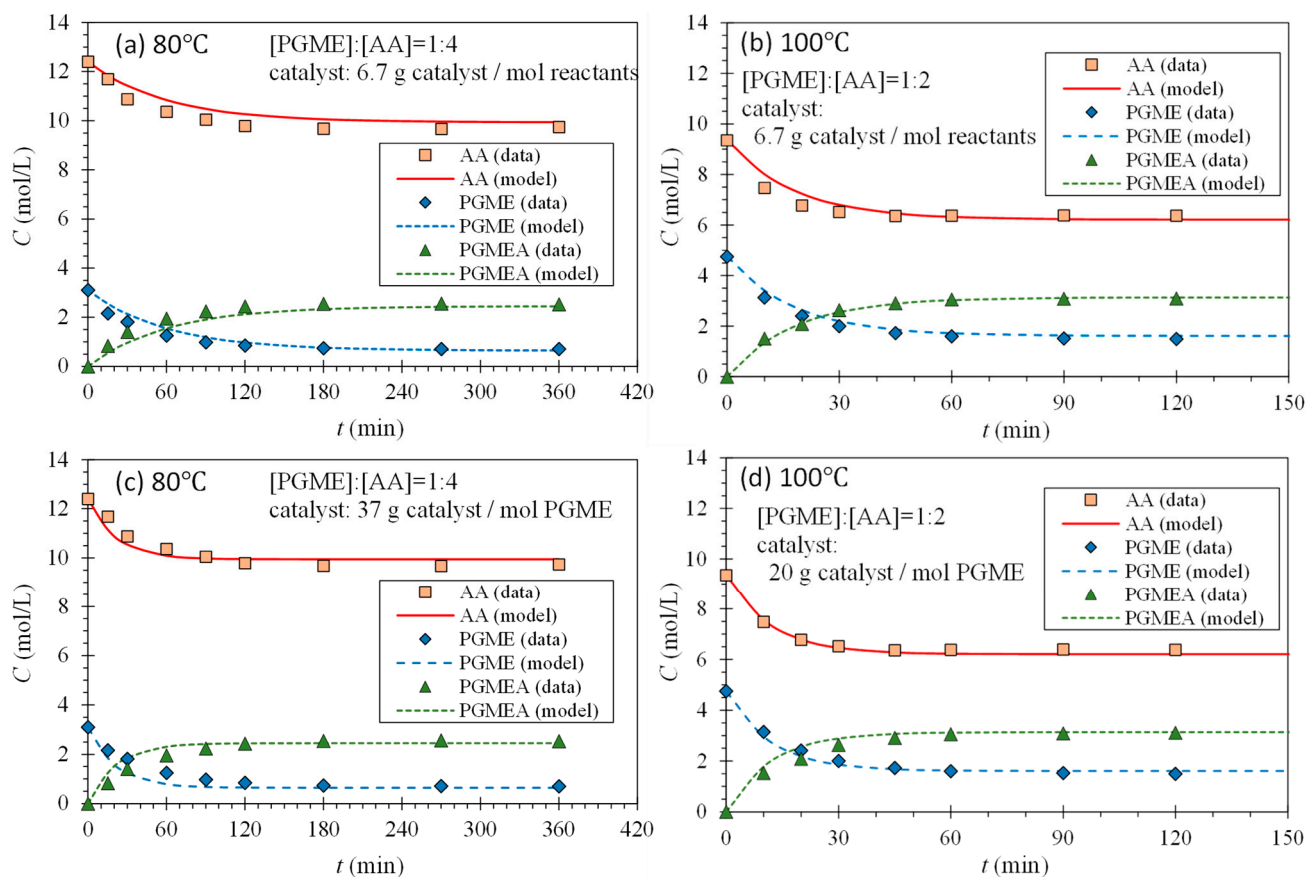

Figure 6. Effects of the molar ratio of reactants and catalyst amount on the concentrations (*C*) of reactants and product with time. The lines represent model predictions, Equations (3) through (9), using the scaled reaction rate constants obtained in the previous section for a 1:1 reactant molar ratio at the relevant temperature. (**a**) [PGME]:[AA] = 1:4 with 6.7 g-catalyst/mol-reactants at 80 °C, (**b**) [PGME]:[AA] = 1:2 with 6.7 g-catalyst/mol-reactants at 100 °C, (**c**) [PGME]:[AA] = 1:4 with 37 g-catalyst/mol PGME at 80 °C, and (**d**) [PGME]:[AA] = 1:2 with 20 g-catalyst/mol-PGME at 100 °C. The absolute amount of catalyst used in (**a**) is the same as that in (**c**), and the absolute amount of catalyst used in (**b**) is the same as that in (**d**).

4.3. Simulation and Data for Plug Flow Reactor System

A plug flow reactor (PFR) presents a practical solution for employing solid catalysts and effectively controlling reaction temperature in chemical processes. In this study, we utilized Aspen Plus 2006.5 to conduct simulations with a reactor model of RPLUG to design a PFR system, incorporating the kinetic parameters obtained from the batch system experiments conducted in this investigation. The simulations were conducted at a temperature of 90 °C, with the bed porosity and density of the catalyst particles set at 0.3 and 0.5 g/cc, respectively. The reactor dimensions were set as a diameter of 0.1 m and a length of 1.5 m. The feed composition was characterized by the mole fractions of

[AA]:[PGME]:[PGMEA] = 0.475:0.475:0.05, with a feed rate of 1.43 kmol/h. Figure 7 illustrates the simulated mole fraction profile for PGME and PGMEA resulting from the PFR design. Notably, equilibrium conditions were achieved within a PFR length of 1.5 m, suggesting that this length represents the minimum requirement for designing a PFR under the specified conditions. This insight allows for an efficient design approach in implementing PFR systems tailored to specific reaction requirements and for showcasing its potential to optimize reactor design while considering variables such as energy cost and manufacturing expenses.
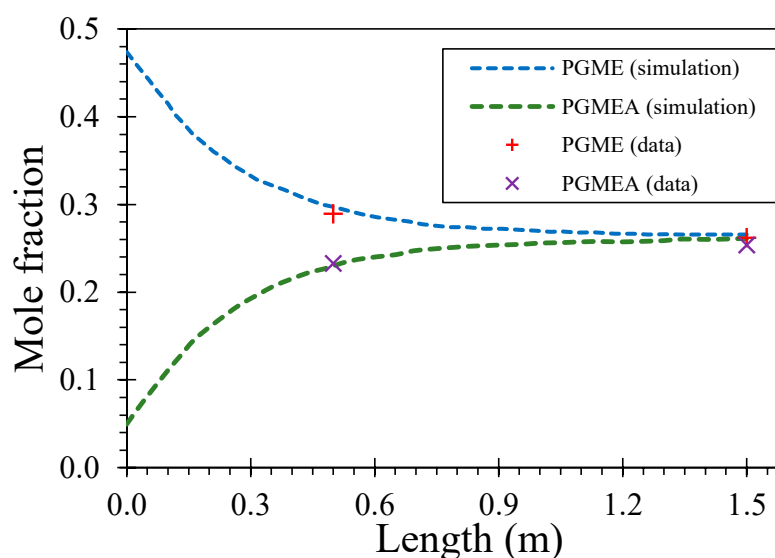
Figure 7. Simulated and experimental mole fraction profiles along with the length of the PFR at 90 °C.

Consequently, a PFR system (Figure 2) was constructed with identical dimensions to those employed in the simulation. To account for the swelling of the catalyst, we swelled the catalyst in deionized water and then filled the PFR reactor with the swollen catalyst up to 1.5 m. By applying the same operational conditions, we determined the mole fractions of PGME and PGMEA at two sampling points within the PFR reactor. These results closely correlate with the simulated outcomes illustrated in Figure 7. Hence, it is apparent that kinetic parameters obtained from batch reactor experiments can significantly contribute to simulation endeavors aimed at designing and constructing alternative reactor configurations. This alignment between simulation results and real-world operation underscores the effectiveness of utilizing such parameters in optimizing the performance of novel reaction systems.

5. Conclusions

Through our study, we conducted the synthesis of PGMEA using AA and PGME alongside a commercially available catalyst, Amberlyst-15. This endeavor aimed to elucidate the critical parameters governing reaction kinetics, alongside the development of an integrated kinetic model. These aspects are both novel and indispensable in the design of other types of reactors. Successfully modeling the reaction kinetics across various temperatures with a 1:1 reactant ratio, we employed an integrated second-order reversible reaction equation along with the Arrhenius model. This approach allowed for the natural determination of kinetic and Arrhenius parameters, pivotal for understanding reaction dynamics. Utilizing these parameters, we extended our analysis to predict reaction kinetics for scenarios involving different reactant ratios and catalyst amounts. Notably, our predictions aligned well with experimental data, particularly when the catalyst amount was scaled by the amount of PGME, the limiting reactant, rather than that of all the reactants.

Interestingly, while the activation energy for the forward reaction mirrored findings from other studies, that of the reverse reaction displayed notable disparities.

Our proposed reaction rate model, coupled with the obtained model parameters, holds significant promise for reactor design and kinetics prediction. For instance, leveraging these insights, we conducted simulations of a plug flow reactor and constructed a PFR system based on the simulation results, showcasing its potential to optimize reactor design while considering variables such as energy cost and manufacturing expenses. In essence, our study contributes to the broader understanding of reaction kinetics and underscores its practical implications in reactor design and optimization.

Supplementary Materials: The following supporting information can be downloaded at https://www.mdpi.com/article/10.3390/pr12050865/s1, Figure S1: Example of chromatogram; Figure S2: Screen capture of conditions for simulation; Figure S3: Flow sheet of simulation for a PFR system with purification processes.

Author Contributions: Conceptualization, Y.R.S. and J.K.P.; methodology: J.K.P. and H.E.P.; software, Y.R.S., J.K.P. and H.E.P.; validation, Y.R.S., J.K.P., E.W.S. and H.E.P.; formal analysis, Y.R.S., J.K.P. and H.E.P.; investigation, J.K.P. and E.W.S.; resources, Y.R.S., J.K.P. and E.W.S.; data curation, Y.R.S., S.P.M. and J.K.P.; writing—original draft preparation, Y.R.S., J.K.P., S.P.M. and H.E.P.; writing—review and editing, Y.R.S. and H.E.P.; visualization, Y.R.S., J.K.P. and H.E.P.; supervision, E.W.S. and H.E.P.; project administration, S.P.M.; funding acquisition, Y.R.S., S.P.M. and J.K.P. All authors have read and agreed to the published version of the manuscript.

Data Availability Statement: Data can be shared upon request. Data are contained within the article.

Conflicts of Interest: Author Seok Pyong Moon was employed by the company Samsung-BP Chemicals. The remaining authors declare that the research was conducted in the absence of any commercial or financial relationships that could be construed as a potential conflict of interest. The [company Samsung-BP Chemicals in affiliation] had no role in the design of the study; in the collection, analyses, or interpretation of data; in the writing of the manuscript, or in the decision to publish the results.

References

1. Hussain, A.; Chaniago, Y.D.; Riaz, A.; Lee, M. Process Design Alternatives for Producing Ultra-high-purity Electronic-Grade Propylene Glycol Monomethyl Ether Acetate. *Ind. Eng. Chem. Res.* **2019**, *58*, 2246–2257. https://doi.org/10.1021/acs.iecr.8b04052.
2. Agrawal, G.; Oh, J.; Sreedhar, B.; Tie, S.; Donaldson, M.E.; Frank, T.C.; Schultz, A.K.; Bommarius, A.S.; Kawajiri, Y. Optimization of reactive simulated moving bed systems with modulation of feed concentration for production of glycol ether ester. *J. Chromatogr. A* **2014**, *1360*, 196–208. https://doi.org/10.1016/j.chroma.2014.07.080.
3. Oh, J.; Sreedhar, B.; Donaldson, M.E.; Frank, T.C.; Schultz, A.K.; Bommarius, A.S.; Kawajiri, Y. Transesterification of propylene glycol methyl ether in chromatographic reactors using anion exchange resin as a catalyst. *J. Chromatogr. A* **2016**, *1466*, 84–95. https://doi.org/10.1016/j.chroma.2016.08.072.
4. Gadekar-Shinde, S.; Reddy, B.; Khan, M.; Chavan, S.; Saini, D.; Mahajani, S. Reactive Distillation for the Production of Methoxy Propyl Acetate: Experiments and Simulation. *Ind. Eng. Chem. Res.* **2017**, *56*, 832–843. https://doi.org/10.1021/acs.iecr.6b03489.
5. Vegh, L. Propylene glycol ethers and propylene glycol ether acetate 'PMA' in coating applications. *Pigment. Resin. Technol.* **1985**, *14*, 4–15. https://doi.org/10.1108/eb042147.
6. Reddy, B.M.; Sreekanth, P.M.; Lakshmanan, P.; Khan, A. Synthesis, characterization and activity study of SO42−/CexZr1−xO2 solid superacid catalyst. *J. Mol. Catal. A Chem.* **2006**, *244*, 1–7. https://doi.org/10.1016/j.molcata.2005.08.054.
7. Zhang, C.; Liu, T.; Wang, H.-J.; Wang, F.; Pan, X.-Y. Synthesis of acetyl salicylic acid over WO3/ZrO2 solid superacid catalyst. *Chem. Eng. J.* **2011**, *174*, 236–241. https://doi.org/10.1016/j.cej.2011.09.010.
8. Shagufta; Ahmad, I.; Dhar, R. Sulfonic Acid-Functionalized Solid Acid Catalyst in Esterification and Transesterification Reactions. *Catal. Surv. Asia* **2017**, *21*, 53–69. https://doi.org/10.1007/s10563-017-9226-1.
9. Sirsam, R.; Hansora, D.; Usmani, G.A. A Mini-Review on Solid Acid Catalysts for Esterification Reactions. *J. Inst. Eng. (India) Ser. E* **2016**, *97*, 167–181. https://doi.org/10.1007/s40034-016-0078-4.
10. Adeeva, V.; Liu, H.Y.; Xu, B.Q.; Sachtler, W.M.H. Alkane isomerization over sulfated zirconia and other solid acids. *Top. Catal.* **1998**, *6*, 61–76. https://doi.org/10.1023/a:1019114406219.

11. Bargujar, S.; Ratnani, S. Aldol condensation: Green perspectives. *J. Iran. Chem. Soc.* **2022**, *19*, 2171–2190. https://doi.org/10.1007/s13738-021-02464-w.

12. Amarasekara, A.S.; Ali, S.R.; Fernando, H.; Sena, V.; Timofeeva, T.V. A comparison of homogeneous and heterogeneous Brønsted acid catalysts in the reactions of meso-erythritol with aldehyde/ketones. *SN Appl. Sci.* **2019**, *1*, 212. https://doi.org/10.1007/s42452-019-0226-9.

13. Fan, Y.; Ye, Q.; Cen, H.; Chen, J.; Liu, T. Novel Process Design Combined with Reactive Distillation and Pressure-Swing Distillation for Propylene Glycol Monomethyl Ether Acetate Synthesis. *Ind. Eng. Chem. Res.* **2019**, *58*, 19211–19225. https://doi.org/10.1021/acs.iecr.9b04122.

14. Chaniago, Y.D.; Nhien, L.C.; Naquash, A.; Riaz, A.; Kim, G.S.; Lim, H.; Lee, M. Pressure Swing-Based Reactive Distillation and Dividing Wall Column for Improving Manufacture of Propylene Glycol Monomethyl Ether Acetate. *Energies* **2021**, *14*, 7416. https://doi.org/10.3390/en14217416.

15. Wang, X.; Wang, Q.; Ye, C.; Dong, X.; Qiu, T. Feasibility Study of Reactive Distillation for the Production of Propylene Glycol Monomethyl Ether Acetate through Transesterification. *Ind. Eng. Chem. Res.* **2017**, *56*, 7149–7159. https://doi.org/10.1021/acs.iecr.7b01462.

16. El-Nassan, H.B. Amberlyst 15®: An Efficient Green Catalyst for the Synthesis of Heterocyclic Compounds. *Russ. J. Org. Chem.* **2021**, *57*, 1109–1134. https://doi.org/10.1134/s1070428021070125.

17. Oh, J.; Agrawal, G.; Sreedhar, B.; Donaldson, M.E.; Schultz, A.K.; Frank, T.C.; Bommarius, A.S.; Kawajiri, Y. Conversion improvement for catalytic synthesis of propylene glycol methyl ether acetate by reactive chromatography: Experiments and parameter estimation. *Chem. Eng. J.* **2015**, *259*, 397–409. https://doi.org/10.1016/j.cej.2014.08.008.

18. Huang, Z.; Lin, Y.; Li, L.; Ye, C.; Qiu, T. Preparation and shaping of solid acid SO42−/TiO2 and its application for esterification of propylene glycol monomethyl ether and acetic acid. *Chin. J. Chem. Eng.* **2017**, *25*, 1207–1216. https://doi.org/10.1016/j.cjche.2016.11.006.

19. Huang, Y.S.; Sundmacher, K. Kinetics study of propyl acetate synthesis reaction catalyzed by Amberlyst 15. *Int. J. Chem. Kinet.* **2007**, *39*, 245–253. https://doi.org/10.1002/kin.20236.

20. Lux, S. Kinetic Study of the Heterogeneous Catalytic Esterification of Acetic Acid with Methanol Using Amberlyst®15. *Chem. Biochem. Eng. Q.* **2016**, *29*, 549–557. https://doi.org/10.15255/cabeq.2014.2083.

21. Pappu, V.K.S.; Yanez, A.J.; Peereboom, L.; Muller, E.; Lira, C.T.; Miller, D.J. A kinetic model of the Amberlyst-15 catalyzed transesterification of methyl stearate with n-butanol. *Bioresour. Technol.* **2011**, *102*, 4270–4272. https://doi.org/10.1016/j.biortech.2010.12.006.

22. Pöpken, T.; Götze, L.; Gmehling, J. Reaction Kinetics and Chemical Equilibrium of Homogeneously and Heterogeneously Catalyzed Acetic Acid Esterification with Methanol and Methyl Acetate Hydrolysis. *Ind. Eng. Chem. Res.* **2000**, *39*, 2601–2611. https://doi.org/10.1021/ie000063q.

23. Yang, J.I.; Cho, S.H.; Kim, H.J.; Joo, H.; Jung, H.; Lee, K.Y. Production of 4-Hydroxybutyl Acrylate and Its Reaction Kinetics over Amberlyst 15 Catalyst. *Can. J. Chem. Eng.* **2008**, *85*, 83–91. https://doi.org/10.1002/cjce.5450850108.

24. Singh, N.; Raj, k.; Sachan, P.K. Kinetic Study of Catalytic Esterification of Butyric Acid and Ethanol over Amberlyst 15. *ISRN Chem. Eng.* **2013**, *2013*, 520293. https://doi.org/10.1155/2013/520293.

25. Xu, Z.P.; Chuang, K.T. Kinetics of acetic acid esterification over ion exchange catalysts. *Can. J. Chem. Eng.* **2009**, *74*, 493–500. https://doi.org/10.1002/cjce.5450740409.

26. Lilja, J.; Aumo, J.; Salmi, T.; Murzin, D.Y.; Mäki-Arvela, P.; Sundell, M.; Ekman, K.; Peltonen, R.; Vainio, H. Kinetics of esterification of propanoic acid with methanol over a fibrous polymer-supported sulphonic acid catalyst. *Appl. Catal. A Gen.* **2002**, *228*, 253–267. https://doi.org/10.1016/s0926-860x(01)00981-4.